

**MSc thesis in
Geoscience and Remote Sensing**

Identification of Neolithic Circular Enclosures through Aerial Imagery

A study about pattern recognition and deep learning techniques

Yuqi Meng, 2022



IDENTIFICATION OF NEOLITHIC CIRCULAR ENCLOSURES THROUGH AERIAL IMAGERY

A STUDY ABOUT PATTERN RECOGNITION AND DEEP LEARNING TECHNIQUES

by

Yuqi MENG

to obtain the degree of Master of Science
in Geoscience and Remote Sensing
at the Delft University of Technology,
to be defended publicly in February, 2023.

Student number: 5256178
Project duration: March, 2022 – February, 2023
Thesis committee: Dr. Roderik Lindenbergh, TU Delft
Dr. Marc Schleiss, TU Delft
John Hefele, cosine Remote Sensing B.V.



ABSTRACT

Traditionally, archaeological investigations, especially archaeological remains detection, mostly depend on human observation. In order to find the objects in large areas, a lot of fieldwork has to be done and it takes a long time for archaeologists to travel around. Nowadays, the development of LIDAR provides accurate 3D geometric information, which can be used for computer-based detailed terrain study. The application of deployment of computer vision methods also provides a new idea for the automatic object detection approach.

In this study, the neural network architecture "ResNet18" was applied to airborne LiDAR data from the Western regions of Slovakia for the automated detection of undiscovered Neolithic Circular Enclosures (also called rondel in the thesis). NCEs are mysterious stone hedge-like rings scattered through Central/Eastern Europe. The LiDAR data was processed into digital raster data and realized data enhancement by the visualization technique – Simple Local Relief Model (SLRM). Since the positive samples were limited, expanding the training dataset was crucial and was realized by data augmentation methods based on the positive samples of rondels. The augmented rondels were created by cropping the real rondels and pasting them on the new empty areas after slight modification. After that, the positive image samples and the same number of negative image samples constructed the whole data set and it was divided into two parts – training data and test data. After the training process of ResNet18, the performances of deep learning models with different combinations of parameters were evaluated, and the selected model was applied to a large area ($44276 \times 29984 \text{ m}^2$), the spatial distribution of the probabilities could be observed and 32 possible new rondel areas were chosen for further validation.

ACKNOWLEDGEMENTS

Firstly, I would like to give my heartfelt thanks to my supervisor Dr. Roderik Lindenbergh for his kindness, illuminating guidance. He also gave me much inspiration each time we had meeting which let me have the courage to face difficult problems during this period. I also would like to express my appreciation to John Hefele from cosine who provided different perspectives for the project and helped me when I had coding problems. Also, I must express my sincere thanks to Dr. Marc Schleiss, who gave my thesis a careful reading, helpful comments and guided me to think deeply.

Sincere gratitude should go to all my Professors from TU Delft for the enlightening lectures and generous help during the years, as well as my classmates who are always kind and ebullient to me.

My acknowledgments also go to my mom, who gave me great love, understanding, comfort and encouragement to support me finished the project and let me become a better person.

I want to thank my friends Fanhao and Jiahua as well for their companionship which made me feel less marooned.

CONTENTS

Abstract	iv
Acknowledgement	vi
1 Introduction	1
1.1 Neolithic Circular Enclosures (NCEs)	1
1.2 Problem statement & Research questions	2
1.2.1 Problem statement	2
1.2.2 Research questions	3
1.3 Thesis Structure	3
2 Literature Review	5
2.1 LiDAR and Point cloud	5
2.2 Visualization techniques	6
2.2.1 Hill-shading	6
2.2.2 Simple Local Relief Model (SLRM)	7
2.3 Deep Learning	7
2.3.1 Introduction to deep learning	8
2.3.2 Convolutional Neural Networks (CNNs)	8
2.3.3 Residual Network(ResNet)	10
3 Dataset	13
3.1 Introduction to Slovakian LiDAR Data	13
3.2 Known Rondels	14
3.3 Pre-processing	15
4 Methodology	19
4.1 Overview of workflow	19
4.2 Data Augmentation	20
4.3 Dataset Construction	21
4.4 The Residual Network Structure	23
4.5 Network Training	23
4.6 Evaluation	23
4.6.1 Cross-Entropy Loss Function	23
4.6.2 Results Classification	24
4.6.3 Probabilities distribution	24
4.7 The comparison group	25

5	Results & Discussion	27
5.1	Results of data augmentation	27
5.2	Running Results and Models	29
5.3	Binary classification results and discussion	30
5.4	Spatial distribution of the prediction results and discussion	32
5.5	Possible new rondels	36
5.6	Results of the comparison group (Evaluate the usefulness of data augmentation)	39
6	Conclusion & Recommendation	43
6.1	Conclusion (Answers to the research questions)	43
6.2	Recommendation for future work.	44
	Bibliography	50
A	Appendix	51
A.1	The architecture of ResNet18	52
A.2	The list of acronym	52

1

INTRODUCTION

In this chapter, the background of our archaeological object of interest, the problem statement and the research questions are presented. This part also provides an overview of the thesis structure.

1.1. NEOLITHIC CIRCULAR ENCLOSURES (NCEs)

Neolithic Circular Enclosures (NCEs) are a kind of mysterious stone hedge-like rings scattered in Europe, especially from the Middle and Late Neolithic period (approximately 7000-4000 B.C.), which are also called rondels (roundels) in Czechia and Slovakia or kreisgrabenanlagen in German [1]. In Central Europe, there are about 120-150 known Neolithic circular enclosures. These earthworks seem to follow a common set of building rules - they generally consisted of 1-4 circular ditches, interrupted by causeways and at least 2 entrances [2]. An example NCE structure is shown in the Figure 1.1.



Figure 1.1: Reconstruction (model) of the Künzing-Unternberg rondel, Museum Quintana, Künzing, Lower Bavaria (800 × 600 pixels)[3].

1.2. PROBLEM STATEMENT & RESEARCH QUESTIONS

1.2.1. PROBLEM STATEMENT

According to current archaeological research, although rondels have some common structure, they have great variability in shape, size and other details. Hence their characteristics can hardly be defined exactly. Moreover, these Neolithic Circular enclosures have experienced different degrees of structural damage in the past few thousands of years. Methods for automatically identifying rondels from aerial images using machine learning could be of great value for future archeological research. However, devising reliable methods can be difficult, since many natural and human-made structures can look like rondels and little information is available about how rondels appear in aerial images. In this project, the digital raster data derived from the airborne LiDAR data is used. In order to realize feature extraction, the raster data needs to be processed into images in several steps.

On the other hand, deep learning is showing the potential of automatic object detection in many fields. It allows automatically features extraction from large amounts of images instead of manually. That's why in this project the research on the viability of the detection of roundels was based on deep learning methods, especially Convolutional Neural Networks (CNNs). One challenge of this approach is that deep learning methods require a large data set for training and feature extraction [4], which is not available in this project. Thus it is necessary to apply an augmentation method to expand the limited amount of positive training examples.

1.2.2. RESEARCH QUESTIONS

Main research question :

- Are CNNs suitable for detecting archaeological features through aerial height imagery based on a limited amount of positive samples?

Sub-questions :

- What are the characteristics of rondels in images acquired by LIDAR?
- How can we train a good NCEs detector given the small size of the training data set?
- What is a good way to measure the performance of the classifier?
- How does the performance vary depending on how the network was trained?
- What's the performance when the model applied to larger areas?
- Can new NCEs be detected using this method?

1.3. THESIS STRUCTURE

The thesis consists of six chapters. **Chapter 1** is the introduction of the project objectives – Neolithic Circular enclosures (NCEs), as well as the research problems and thesis structure. **Chapter 2** presents the published work involving the main methods used for the approach in this research, which contains introduction of LiDAR data, methods for data pre-processing and deep learning neural networks. **Chapter 3** presents the details about the introduction of data used in this project and the pre-processing application prepared for following operations. **Chapter 4** is the part about methodology, which shows the workflow and more details about the main process to achieve the research objectives. In **Chapter 5**, the results for each of the main steps are shown, and the results are discussed and analyzed. In addition, several possible new rondels are selected for further verification. **Chapter 6** concludes the answers to the research questions and gives recommendations for future work.

2

LITERATURE REVIEW

In this chapter, different concepts and methods related to the research objectives are introduced based on the previous work. In section 2.1, there are basic principles to the LiDAR system, as well as its output – point clouds. In section 2.2, two visualization techniques and their methods are introduced. In section 2.3, there is an introduction to deep learning networks and their wide use in the research area in recent years.

2.1. LiDAR AND POINT CLOUD

LiDAR is the abbreviation of "Light Detection And Ranging". It is a remote sensing technology for the acquisition of 2.5D data [5] by using a laser and recording the reflecting time from the laser to the object. Because the speed of light is known, the range from the sensor to the object can be measured by the product of the speed of light propagation and the travel time. The computation is shown as equation 2.1, in which "d" represents distance between sensor to target, "c" represents the speed of light, and "t" represents the travel time.

$$d = \frac{ct}{2} \quad (2.1)$$

A LiDAR system including a laser, a scanner and a GPS receiver [6]. Based on different scanner platforms, LiDAR applications can be divided into space-borne, terrestrial, airborne types [7]. Airborne LiDAR platforms like airplanes and helicopters are the most common LiDAR systems [6]. The output of a LiDAR system is a 3D points collection called a "point cloud". A point cloud has the information about X,Y coordinates and the elevation (Z), the intensity of each point and sometimes the classification of the LiDAR data [8]. The LiDAR data is applied increasingly to archaeology, because the output products from the LiDAR can be used for deriving high-resolution elevation models and extracting 3D Earth surface features [9].

2.2. VISUALIZATION TECHNIQUES

In recent years, the development of high-resolution digital topographic data is becoming more valued for automatic detection of archaeological features, instead of human observation [10]. The original point cloud LiDAR data was processed into Digital Terrain Model (DTM) and Digital Surface Model (DSM) raster data [11]. Elevation features of rondels can be helpful for automated detection because of the presence of circular features in the elevation due to the ditches.

Applying a visualization technique to LiDAR data to enhance terrain is a promising approach for characteristics extraction of rondels. There are various visualization techniques, such as Hill-shading, Simple local relief model, Sky-view factor etc [12]. Each one of them has its strengths and weaknesses in usability and efficiency [13]. According to an earlier study, the hill-shading is the most common visualization technique of archaeological landscapes [14]. Simple Local Relief Model is considered the most useful for raster elevation data [14]. Thus, we applied and compared the performance of these two visualization techniques – hill-shading and Simple Local Relief Model (SLRM) based on the elevation model raster dataset.

2.2.1. HILL-SHADING

Hill-shading (also known as relief shading or shaded relief) [12], is a technique for visualizing terrain by simulating the effect of natural light on the elevation surface according to the intensities of reflected light at the land cells, as shown in Figure 2.1. Hill-shading creates three-dimensional surfaces from a two-dimensional display.

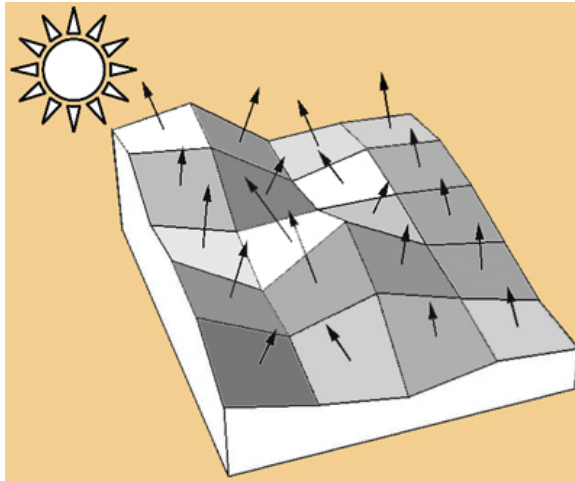


Figure 2.1: Formation of a hill-shade image [15].

Depending on the angle of incidence, hill-shading can be divided into two categories:

traditional hill-shading and multi-directional hill-shading [15]. While traditional hill-shading calculates mountain shadows from a fixed single light source direction, the multi-directional method can calculate mountain shadows from multiple light source directions [15]. Compared with the single light source hill-shading technique, the light from multiple sources can be fused to enhance the visualization of the terrain, since it overcomes the inability of representing linear objects parallel to the direction of the light source, as well as the saturation of shadow areas[14].

2.2.2. SIMPLE LOCAL RELIEF MODEL (SLRM)

SLRM is a visualization technique used for creating "difference maps". The basic idea of SLRM is to generalize the terrain surface by subtracting the smoothed surface and getting a small-scale local elevation difference map [14]. The new model highlights archaeological features and removes the influence of the natural landscape. Therefore SLRM is considered the most efficient model to visualize elevation raster data [16]. Moreover, since small-scale local elevation difference maps can be used for exploring possible structures of earthworks, SLRM is one of the most useful models for archaeological prospection [17].

The first main step of SLRM creation is to create a smoothed surface by using a low pass filter based on a fixed circular neighborhood radius, then subtract the differences between the original elevation model and the normalized surface. That's how we get the final difference map [18]. An example of such final difference map is shown in Figure 2.2

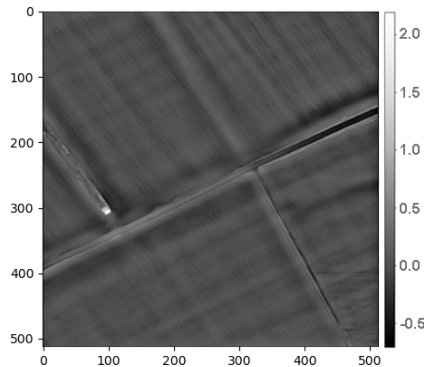


Figure 2.2: A SLRM difference map based on DTM raster data.

2.3. DEEP LEARNING

In recent years, deep learning approaches are being progressively used for the automatic detection of archaeological objects, especially deep learning convolutional neural

networks (CNNs).

2.3.1. INTRODUCTION TO DEEP LEARNING

Deep learning is a subdomain of the machine learning. Machine learning algorithms are trained on examples to learn a task in a similar fashion to how humans learn. In this way, the computer can learn to perform classification or detection tasks directly from images, text or other kinds of samples [19]. Models are trained according to labeled data. A neural network contains three kinds of layers – an input layer, hidden layers and an output layer, of which the structure is shown in Figure 2.3. The number of hidden layers can vary depending on the problems. Traditional neural networks only consist of several hidden layers, but deep learning neural networks can contain hundreds of hidden layers, which increases the complexity of automatically features extraction[19]. Thus, some of the models show much better results than ever before. That's why deep learning methods are getting more and more attention in many research fields in recent years.

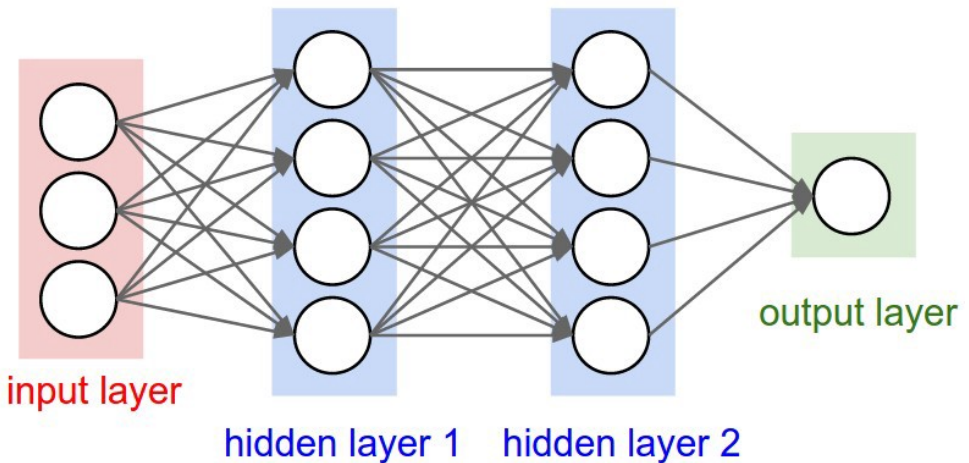


Figure 2.3: The structure of Neural Networks [20].

2.3.2. CONVOLUTIONAL NEURAL NETWORKS (CNNs)

CNN is a specialized type of artificial neural network that uses a mathematical operation – convolution in the layers [21]. It was first popularized by Yann LeCun, for hand-written digits images classification [19]. As a multi-functional solution, CNNs can work well when large amounts of data is available.

In CNNs, convolution operations are applied in the input and hidden layers. These layers convolve the input matrix by convolution kernels and create the feature map by sliding the convolution kernel along the input matrix, then the feature map is passed to the next layer. Moreover, there are other layers called pooling layers (aggregate

the characteristics of different locations by pooling operations, such as max pooling or average pooling), fully connected layers (turning feature map matrix into a single column), etc [21]. The basic architecture of CNNs is shown in Figure 2.4.

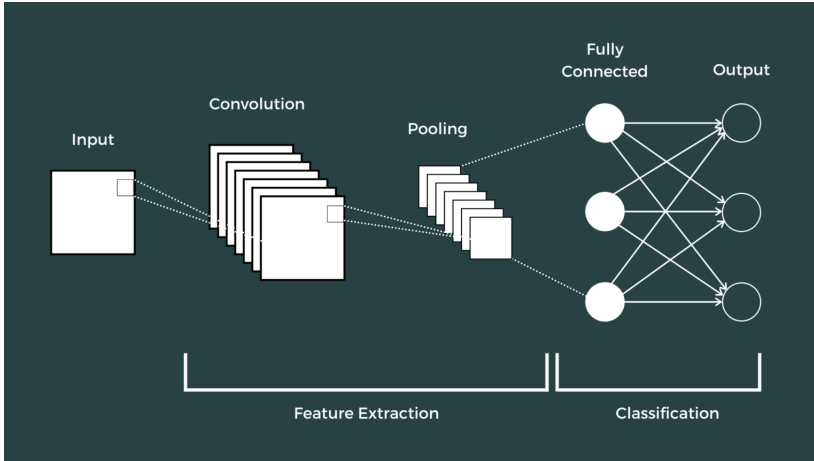


Figure 2.4: The structure of Convolutional Neural Network [22].

The pattern and shape recognition ability of CNNs is valued and widely used, which makes them the standard algorithm used for object detection tasks [23]. According to [23], most machine learning methods can only use the shape of single-row vectors of inputs. However CNNs are able to use the multi-dimensional shape matrices of the inputs and extracts characteristics for landmarks in multiple directions. That's why CNNs show more sensitivity for pattern recognition in images.

As for the limitation of CNNs, on the one hand, the visualized quality of the archaeological data varies which adds uncertainty to feature extraction in CNNs. Additionally, the amount of archaeological data is generally not large enough for effective training [10]. These caused difficulty in the effectiveness of CNNs.

There is a variety of deep learning networks based on CNNs. Recently, one of the most famous algorithms for object detection is called YOLO (You Only Look Once) [24]. It is popular because of its high speed and accuracy. Figure 2.5 shows an example structure of YOLO.

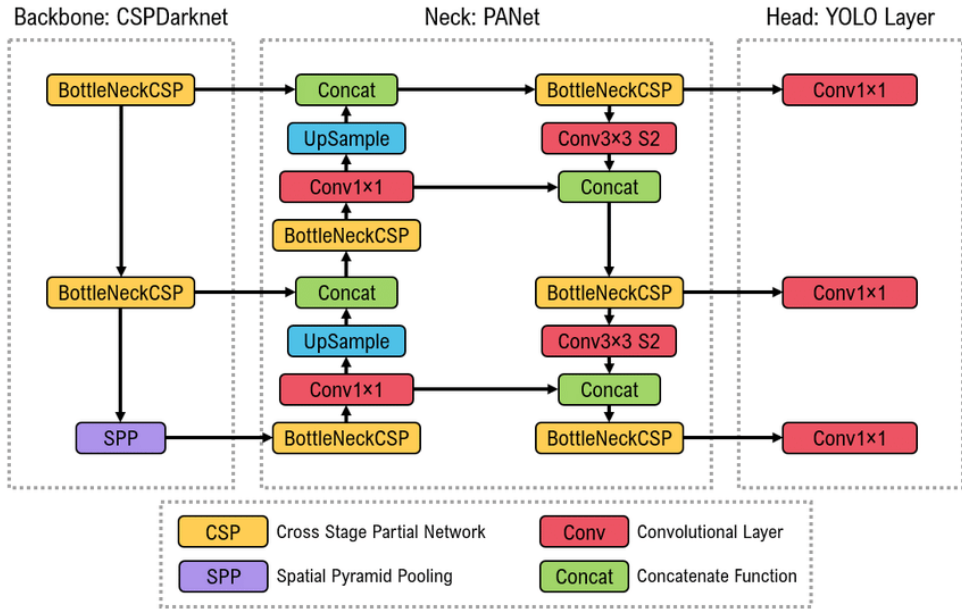


Figure 2.5: The structure of YOLOv5 [25].

For application, firstly we should draw bounding boxes for training images in software and generate the class text file automatically [26]. After classification, the outputs of YOLO are the new bounding boxes for images, the score of the class possibility and the labels. YOLO can be an extremely fast and high-accuracy algorithm in some situations, but also has limitations. In this project, We avoided drawing bounding boxes because there was no way guarantee that they would be drawn consistently. Thus we consider using another network – ResNet (Residual Network).

2.3.3. RESIDUAL NETWORK (RESNET)

Residual Network was created in 2016 as a method that adds the residual block into the neural networks to allow the efficient training of deeper networks [27]. During the general training process, the accuracy should increase with the depth of the layers. However, it is found that the accuracy will saturate at a certain point and then begins to decrease with the depth increase of layers [28]. That causes hard training problems. That's why the residual block is used.

The residual block contains two parts: the main path and the skip connection. If the input is x , the output - desired mapping is $H(x)$. In the residual networks, the layers fit the residual mapping $F(x)=H(x)-x$ instead of fitting the ideal mapping $F(x)$ directly, and then add the learned residual information to the original output. The residual mapping is often easier to optimize in practice. When the residual is 0, the network is an identity mapping from x to $F(x)$, as shown in Figure 2.6. The output from one layer skips several

layers in the identity block. It is easy to learn the identity mapping, which can ensure that the performance of the original network will not be affected after being deepened.

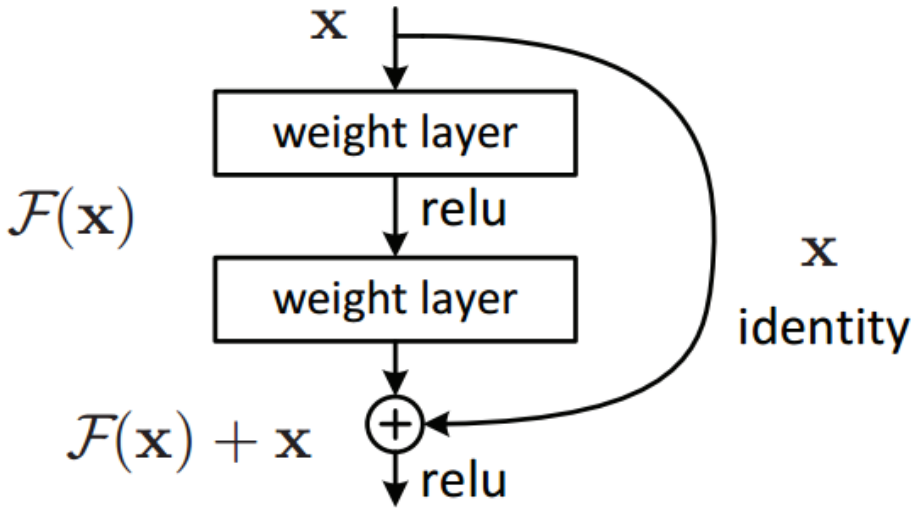


Figure 2.6: The Residual Block (identity block)[27]

Because of the realization of identity mapping in ResNet, the increase of layers will not reduce the network performance, which allows us to train deeper networks [28]. In our project, I will use ResNet18 for the classification task, the example ResNet18 architecture which has 1000 classes (1000 means the total number of scene and object categories in photographs according to [29]) is shown in Figure 2.7.

There are 17 convolutional layers and one fully-connected layer, which generates the "18" in ResNet18 [28]. In practice, a Softmax layer is usually added afterward to present the probability of each class. ResNet18 has a simpler structure and is easier to be modified without worrying about the "Vanishing Gradients" problem. More details of the parameters of the network will be shown in chapter 4.

Layer Name	Output Size	ResNet-18
conv1	$112 \times 112 \times 64$	$7 \times 7, 64, \text{stride } 2$
conv2_x	$56 \times 56 \times 64$	$3 \times 3 \text{ max pool, stride } 2$ $\left[\begin{array}{c} 3 \times 3, 64 \\ 3 \times 3, 64 \end{array} \right] \times 2$
conv3_x	$28 \times 28 \times 128$	$\left[\begin{array}{c} 3 \times 3, 128 \\ 3 \times 3, 128 \end{array} \right] \times 2$
conv4_x	$14 \times 14 \times 256$	$\left[\begin{array}{c} 3 \times 3, 256 \\ 3 \times 3, 256 \end{array} \right] \times 2$
conv5_x	$7 \times 7 \times 512$	$\left[\begin{array}{c} 3 \times 3, 512 \\ 3 \times 3, 512 \end{array} \right] \times 2$
average pool	$1 \times 1 \times 512$	$7 \times 7 \text{ average pool}$
fully connected	1000	$512 \times 1000 \text{ fully connections}$
softmax	1000	

Figure 2.7: An example architecture of ResNet18 [29].

3

DATASET

In this chapter, the details of the LiDAR data and the rondels are introduced, as well as the main pre-processing operations on the data. This part is the cornerstone of Chapter 4.

3.1. INTRODUCTION TO SLOVAKIAN LiDAR DATA

The project is applied to image generated from airborne LiDAR data from the Western regions of Slovakia. The LiDAR data was created by the Geodesy, Cartography and Cadastre Authority of the Slovakia Re-public (ÚGKK SR), which was collected as a point cloud via Airborne Laser Scanning. The coverage of the data is shown in Figure 3.1.

The original point cloud LiDAR data was processed into Digital Surface Model (DSM) raster data and Digital Terrain Model (DTM) raster data [11]. The DTM/DSM raster data are 2.5D elevation models derived from the LiDAR point cloud. DTM is the digital expression of topographic information with spatial position features and terrain attribute features. DSM is an elevation model which includes the height of landmarks, such as buildings, bridges and trees [30]. LiDAR DTM/DSM data in our project are shown in Table 3.1. The basis for the work is from a preliminary study by Eric Prehn [11], a master student from Leiden University. He has already worked on the pre-processing of the LiDAR data such as visualization techniques selection and preliminary data augmentation for the following archaeological purposes.

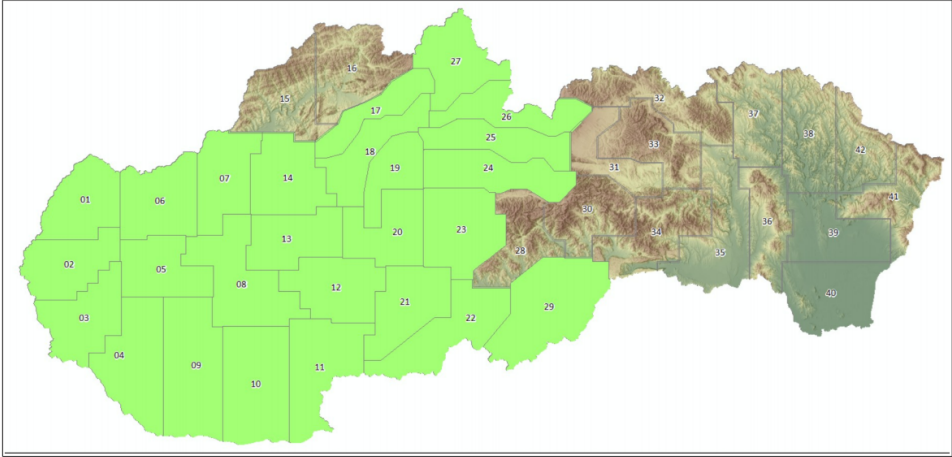


Figure 3.1: The coverage of the Slovakia LiDAR data for this project (The green parts of the map: LOT01 to LOT29 without LOT15, LOT16 and LOT28). Slovakia was divided into 42 parts and was numbered from LOT01 to LOT42. (source of the map: [11])

Attribute	Detail
Provider and Owner	Geodetic and Cartographic Institute Bratislava (GKÚ)
Source Reference	ÚGKK SR
Ground Sampling Distance (GSD)	1 m/pixel
Format	TIFF + TFW
Number of channels	1
Coordinate reference system	ETRS89-TM34+hETRS89 -EPSG code:3046

Table 3.1: Details of LiDAR DTM/DSM data (source: [11]). The full name of ÚGKK SR is "Úrad geodézie, kartografie a katastra Slovenskej republiky" [31], which means the Office of Geodesy, Cartography and Cadastre of the Slovak Republic.

3.2. KNOWN RONDELS

In the research area – the Western regions of Slovakia, there are 35 known rondels, which are numbered from "Slovakia 1" to "Slovakia 35" [11]. The rondels have a common set of building rules - they consisted of 1-2 circular ditches interrupted by causeways and each of the ditches is nearly 80–200m in diameter. Their existence has been verified by archaeologists in Slovakia. Their locations were extracted through the open source Geographic Information System software – Qgis [32]. After that, the visualization techniques were selected to derive images for data set construction later.

3.3. PRE-PROCESSING

As mentioned in Section 2.2, two visualization techniques were applied – Hill-shading and Simple Local Relief Model (SLRM). Moreover, the techniques were applied to two types of data – Digital Terrain Model (DTM) and Digital Surface Model (DSM) raster data. The DTM raster data is used to express topographic information. The DSM raster data was also used because some rondels may have on-surface remains or the vegetation around the rondels may have distinctive features through airborne data. That's why it is also worth visualizing these parts for rondel detection.

3

For hill-shading, altitude and azimuth are the most important characteristics for building the 3D model, as shown in Figure 3.2. Altitude is the solar elevation angle above the horizon and azimuth is the relative position of the sun along the horizon (in angular units) [33]. In this project, the altitude is 45 degrees and azimuth is 315 degrees from the northwest (these are standard settings according to [14]). Some hill-shading images are shown in Figure 3.3.

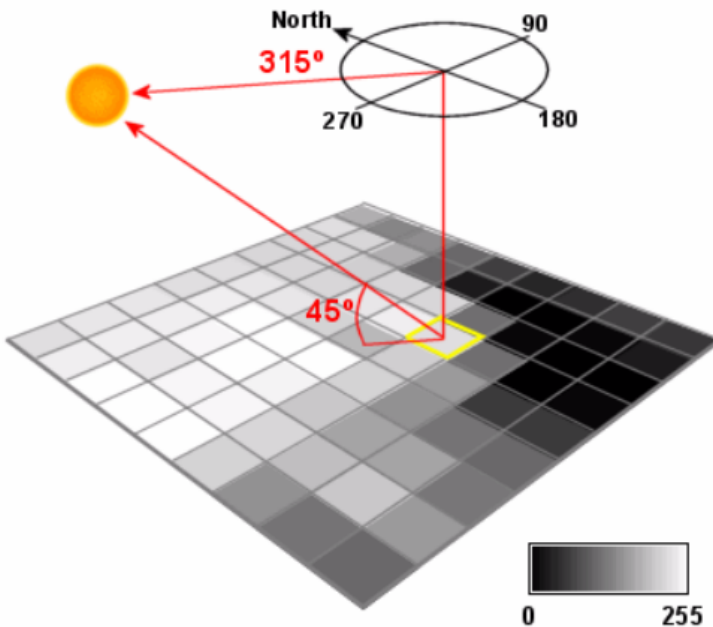
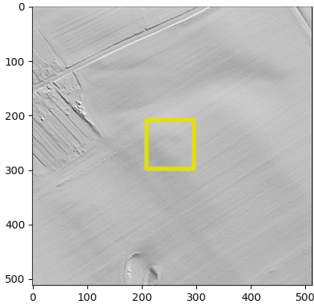
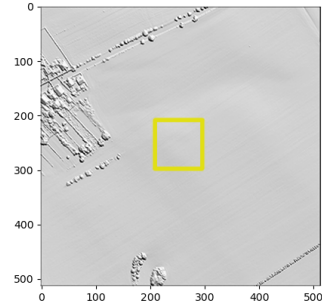


Figure 3.2: Creating a hill-shading from the topographic model [34].



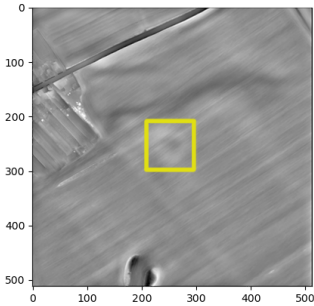
A hill-shading image based on DTM data.



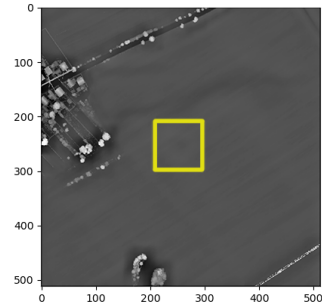
A hill-shading image based on DSM data.

Figure 3.3: Hill-shading images of a rondel (the rondel is in the middle of the images in the bounding boxes).

For SLRM, the most important parameter is the radius for trend assessment in pixels [35]. In this case, the value of the radius was set as 20, which means that the average cell elevation is based on the 20 nearest pixels (20 meters). Next this the average elevation was subtracted from the cells. Two examples of SLRM images are shown in Figure 3.4.



A SLRM image based on DTM data.



A SLRM image based on DSM data.

Figure 3.4: SLRM images of the same rondel as shown in Figure 3.3 (the rondel is in the middle of the images in the bounding boxes).

When we compare the 4 images in Figures 3.3 and 3.4, it is obvious that the SLRM image based on the DTM raster data shows the best visualization, because the rondel looks the clearest in the image. Therefore all 35 rondels were derived by SLRM and hill-shading techniques based on the DTM and DSM raster data. The results showed that the SLRM-DTM data had the best visibility. From the 35 rondels, 20 of them are visible to the naked eyes. The 20 images and their corresponding identifiers are shown in Figure 3.5. Based on the 20 selected rondels, we used an augmentation method to expand the limited training data set.

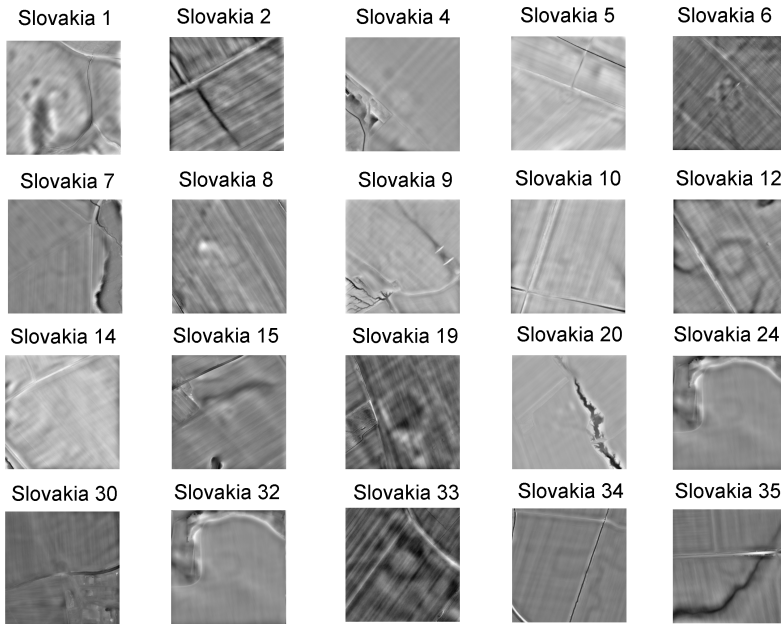


Figure 3.5: The 20 visible rondel images derived by SLRM based on the DTM raster data (all of them are 512×512 pixels).

4

METHODOLOGY

This chapter presents the methodology of this project.

4.1. OVERVIEW OF WORKFLOW

The workflow of the project is shown in figure 4.1. It is divided into 5 main color coded parts. Then more details will be provided in the following sections.

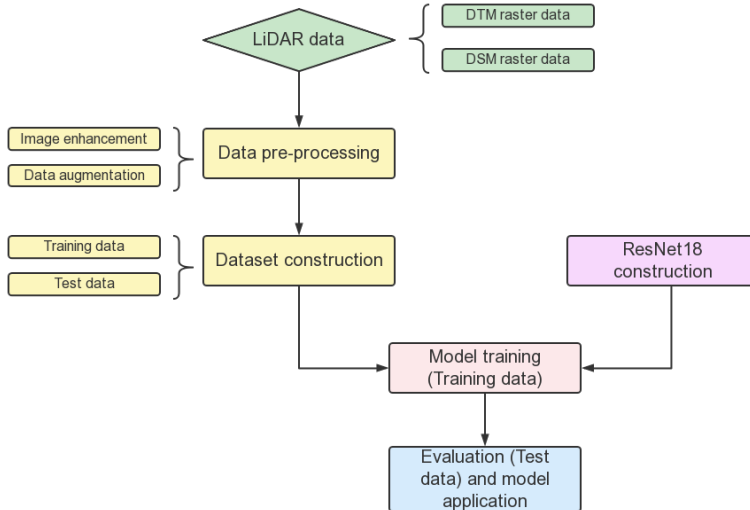


Figure 4.1: Overview of workflow.

4.2. DATA AUGMENTATION

A schematic of augmentation is shown in Figure 4.2. Augmentation is divided into these steps:

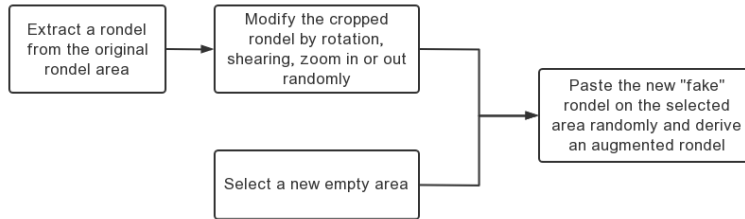


Figure 4.2: The process of creating one augmented rondel.

Step 1 First the rondel is cropped from the original area. Considering the variety of the sizes of different rondels, the bounding boxes were set up for rondels. An example of the original rondel and the cropped rondel is shown in Figure 4.3.

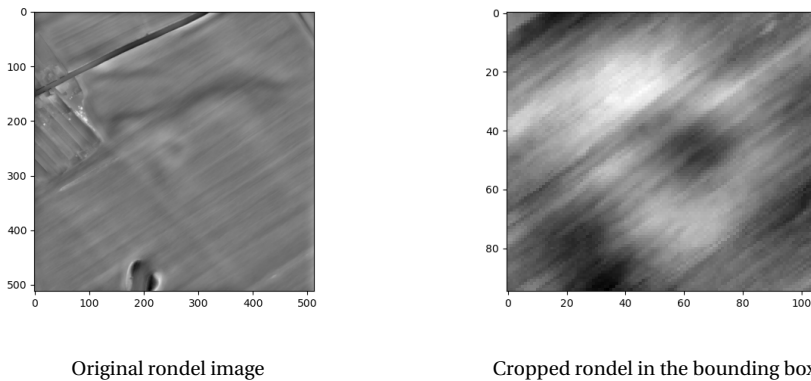


Figure 4.3: The first step.

Step 2 Secondly, the empty areas were chosen for pasting augmented rondels. An "Empty area" means an area without rondel. In order to expand the data set, 50 empty areas were chosen for each original rondels.

Step 3 The cropped rondels were modified slightly and the new "fake" rondels were pasted on the empty areas. That's how we get augmented rondels.

Step 4 During the application of the process, the last step is to select useful augmented rondels. In step 2, "fake" rondels might be pasted on areas with channels, roads, rivers,

or houses. For example, in Figure 4.4, there are 9 augmented rondels based on Slovakia 15, which are numbered from 15-1 to 15-9. After selection, only augmented rondel 15-4, 15-5, 15-7, 15-9 were selected to build the dataset.

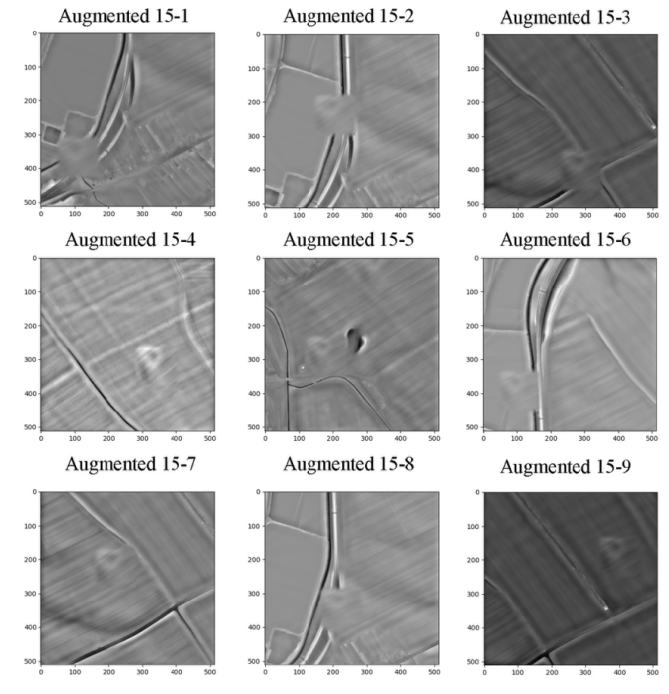


Figure 4.4: The 9 augmented rondels of Slovakia 15 Among the images, the augmented rondels 15-4, 15-5, 15-7, 15-9 were approved as training data. Other "fake" rondels positioned on the channels, roads or water areas and can not be used.

4.3. DATASET CONSTRUCTION

The construction of the data set is crucial to the performance of the network. Generally, the data set is randomly split into "training data" and "test data" [36]. The training data is used for training a model, the test data is used for evaluating the model performance.

However, test data should be independent of training data to avoid data leakage [36]. In this project, the augmented rondels are the replicas of the real rondels, if one real rondel and its augmentation exist in different file folders (training folder and test folder), the accuracy of test data will be higher than the true value. That's why the real rondel and their augmented rondels were put together.

As for the negative dataset, the same number of negative samples as the positive ones was used. This structure makes positive and negative data set have a balanced number of samples. The negative samples are from the other areas of Slovakia which have no

rondel. In general, the ratio of positive and negative samples should be the same as the actual situation. However, in this project, there are only a few rondels in Slovakia, which means the number of negative samples is far more than the positive ones. If the real ratio in reality was used, there is a large probability that the computer ignores the rondel and fails to extract the features from the rare objectives. If the real ratio was used, even if there were many examples of rondels, the optimization algorithm could still decide to minimize just by calling everything negative. According to the related work, feeding the classifier with unbalanced data may make it biased towards the majority of classes, because it did not have enough data to learn from the minority classes [37]. When facing classification problems on rare objectives, similar proportions of positive and negative samples are recommended. The experiments in [38] and [39] can also indicate that the balanced data produces the highest balanced accuracy. Although there are some disputed opinion on it, it is the most common setting for binary classification problem. That's why the positive and negative samples are balanced in quantity in this project.

Thus, the data structure was set up as figure 5.2.

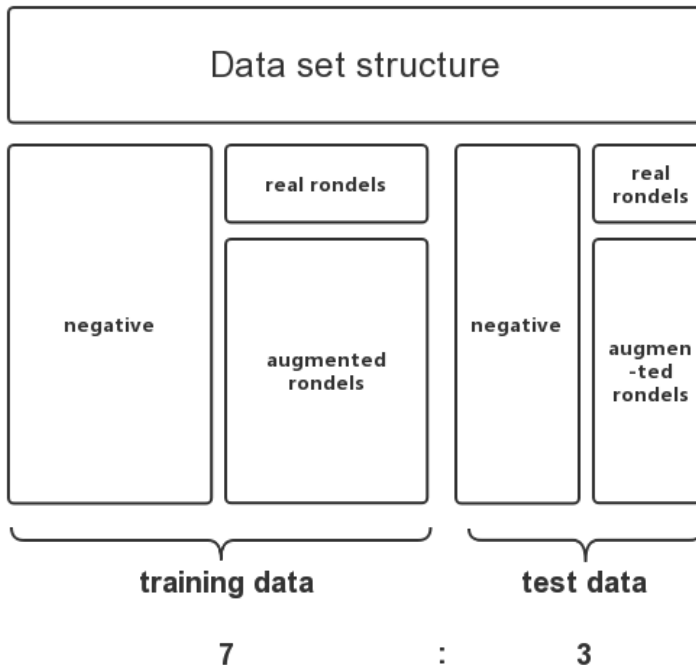


Figure 4.5: The structure of the traing and test data set.

4.4. THE RESIDUAL NETWORK STRUCTURE

The Residual network was built according to the structure shown in Figure A.1 using Pytorch A.1, the Residual Network was built using Pytorch [40]. There are 5 blocks, one fully connected layer, and one softmax layer in the network. The first block is a block with convolutional layers. From block-2 to block-5, each of them consists of 2 residual blocks, and each of the residual blocks has 2 convolutional layers. For the network, the inputs are images with fixed size – 224×224 pixels. And the outputs of the softmax layer are the probabilities of the rondel existence.

4.5. NETWORK TRAINING

After building up the deep learning network, the next step is training the network. At the beginning of the training process, the input images were normalized in fixed size and transformed into tensors. Then the tensors were fed to the network. To improve the running speed of training, a GPU server was used. 300 epochs were used in the process.

There are several essential parameters controlling the training process. The values of batch size, initial learning rate, as well as the different kinds of optimizers were modified to observe the influence on their performance.

- Batch size: Batch size is the number of samples in one iteration [41]. If the batch size is too small, it is hard to converge. If the batch size is too big, it is hard to learn details. The values of batch size were 16, 32, and 64 in this project.
- Initial learning rate: The initial learning rate must have an optimal value. If it is too small, the model will converge slowly or cannot learn. If it is too large, the model will not converge. The initial learning rates were 0.01, 0.001, and 0.0001 in this project.
- Optimizer: 2 optimizers were applied for training – SGD (Stochastic Gradient Descent) and Adam (Adaptive moment estimation) [42].

4.6. EVALUATION

4.6.1. CROSS-ENTROPY LOSS FUNCTION

To measure the performances of training results, the Cross-Entropy Loss Function was used. The function calculates the difference between the model's prediction and the actual probabilities, as shown in Function 4.1 [43]. That's why it is used for performance evaluation in this research when the probabilities of rondels are given out. In the function, "p" means the real probability(which is 1 or 0 in this project), and "q" means the predicted probability. Lower value of loss represents better performance of model.

$$H(p, q) = -\frac{1}{n} \sum_{i=1}^n p(x_i) \cdot \log q(x_i) \quad (4.1)$$

For each epoch, the value of test accuracy is computed by the ratio of the right prediction to total prediction [44]. The loss and accuracy are complementary and essentially the

same, so they have an opposite trend. They can be used for evaluating the performance of the network for each model, the changing values of test loss and accuracy can also be observed in these ways.

4.6.2. RESULTS CLASSIFICATION

In order to evaluate the performance of classifier, the threshold was set to 0.5 (or 0.75) for results testing. If the probability is larger than 0.5 (or 0.75), the test image is regarded as containing a rondel. If the probability is smaller than 0.5 (or 0.75), a image is regarded as the one without rondel. Thus the accuracy of the model can be calculated by the equation 4.2 [44]. In this project, the number of rondels is small in the large area. If a large number of empty areas are predicted as areas with rondels by the model, humans will have to spend a lot of time checking the potential sites. That's why the number of true positives and false positives is essential for model performance evaluation, especially the number of false positives, which should be as small as possible (while keeping the ability to actually detect some of the rondels). The precision of the model is calculated by the equation 4.3 [44]. Moreover, based on the classification results, the number of true positives (TP), true negatives (TN), false positives (FP) and false negatives (FN) can be observed and use to create the confusion matrix which is shown as Table 4.1.

$$Accuracy = \frac{TP + TN}{All} \quad (4.2)$$

$$Precision = \frac{TP}{TP + FP} \quad (4.3)$$

	Predicted	
Actual	Positive	Negative
Positive	TP	FN
Negative	FP	TN

Table 4.1: The confusion matrix.

4.6.3. PROBABILITIES DISTRIBUTION

On the other hand, setting the threshold value may not be the best way to evaluate the results. The distribution of probabilities over a large area can also be an effective way to reflect the performance of the model. That's why the selected model was applied on a larger area and the spatial distribution of the probabilities was observed. As mentioned, the research area contains 26 parts. The model was particularly applied on the area numbered "LOT05", because here most roundels - 7 rondels are located(Figure 4.6). According to the combination of possibilities and naked eyes, possible new rondels can be selected for further validation.

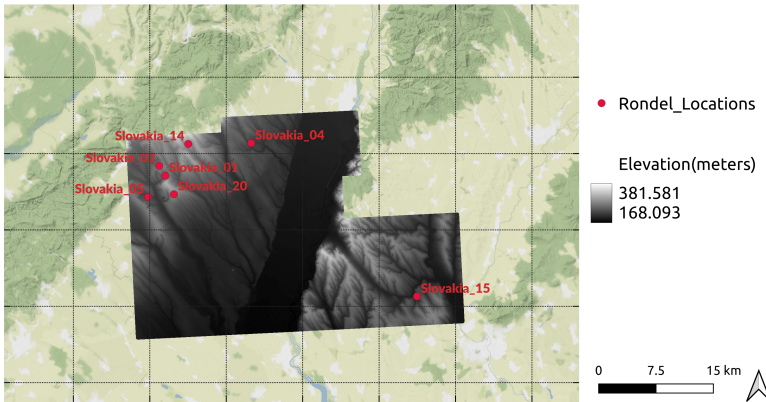


Figure 4.6: The DTM map and location of rondels on LOT05.

4.7. THE COMPARISON GROUP

According to the publications, generally CNNs can work well when large amounts of data is available. That's why the number of positive samples was expanded, considering the limited number of real rondels in this project. However, when the original rondels were cropped and pasted on the new areas, there was a possibility that the original geographic characteristics lost in the process and this would result in information loss and produce a worse model. In order to evaluate the usefulness of data augmentation, a comparison group was created with a training data set without augmented rondels. In this data set, all the 20 real rondels are used for training. Thus the new training data set has 40 samples. Half of them are positive samples and the other ones are negative samples. After the training process, the new model will be applied on the previous selected possible new rondels. The new probabilities would come out and be used for comparison.

5

RESULTS & DISCUSSION

In this chapter, the results are shown, and discussed. The possible new rondels are selected for further verification.

5.1. RESULTS OF DATA AUGMENTATION

According to the methods and steps discussed in Section 4.2, 50 new empty areas were chosen for creating augmented rondels for each original rondel. The augmentation examples are shown in Figure 5.1. The input of the augmentation are the 20 original rondels, 1000 new empty areas (50 for each original rondel), and the bounding boxes. The output consists of the augmented rondels. The numbers of obtained augmented rondels are shown in Table 5.1. Then the results are ready for training and test data construction for CNNs.

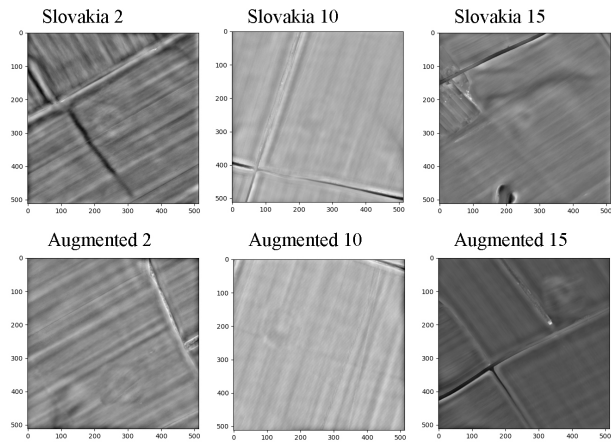


Figure 5.1: Examples of data augmentation.

5

	Number of augmented rondels
Slovakia 1	29
Slovakia 2	28
Slovakia 4	20
Slovakia 5	35
Slovakia 6	20
Slovakia 7	22
Slovakia 8	25
Slovakia 9	19
Slovakia 10	30
Slovakia 12	16
Slovakia 14	22
Slovakia 15	24
Slovakia 19	14
Slovakia 20	19
Slovakia 24	4
Slovakia 30	27
Slovakia 32	13
Slovakia 33	19
Slovakia 34	19
Slovakia 35	16
Total	421

Table 5.1: The numbers of augmented rondels based on 20 original rondels.

Based on the augmentation results and the method mentioned in section 4.3, the data

set was created for the following training and test process in CNNs.

At first, the 20 rondels were divided into 2 parts. The ratio is 7:3, which means 14 rondels for training and 6 rondels for test were used. Then the corresponding augmented rondels were added to the positive data set. In addition, I choose 337 samples from the negative data. In this way the negative samples and positive samples are the same in number, and the training data set consists of 674 samples. On the other hand, the test data set has the same construction as the training one. Thus the whole data set has 882 samples, the structure can be shown in Figure 5.2.

Data Set (882)			
Training (674)		Test (208)	
positive (337)	negative (337)	positive (104)	negative (104)
Slovakia 1, 2, 4, 5, 6, 7, 8, 9, 10, 12, 14, 15, 19, 20 (14)	Negative samples derived from area without rondels (337)	Slovakia 24, 30, 32, 33, 34, 35 (6)	Negative samples derived from area without rondels (104)
Corresponding augmentation (323)		Corresponding augmentation (98)	

Figure 5.2: The structure of the dataset.

5.2. RUNNING RESULTS AND MODELS

Different combinations of characteristics result in different models and their performances. By applying the cross-entropy loss function during the process, the model performances on the test data set can be shown in Figures 5.3 and Table 5.2. When comparing the test loss of three models with different batch-size, the 32 batch-size model shows the lowest loss. For models with 0.01, 0.001 and 0.0001 initial learning rate values, the one with 0.001 shows the best performance. Moreover, the model with SGD optimizer has a more stable performance than the one with Adam optimizer. To sum up, the model with 32 batch-size, 0.001 initial learning rate and SGD optimizer shows the lowest loss, which means the best performance on the test data set.

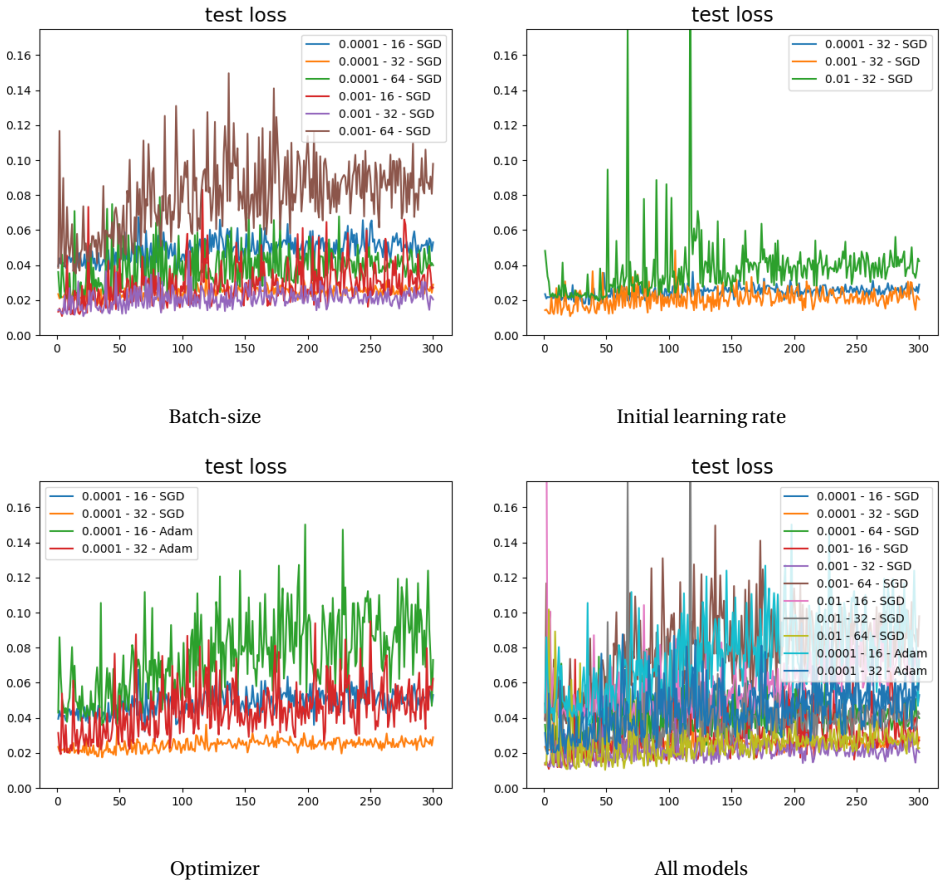


Figure 5.3: The loss of models with different characteristics combinations (The x axis represents loss and the y axis represents epochs).

5.3. BINARY CLASSIFICATION RESULTS AND DISCUSSION

In this section, it is assumed in advance that all rondels in the area have already been detected and there are no more rondels. When the best model was applied for detecting rondels, it returned the probability that a rondel was present in the image. Firstly, the probability threshold was set to 0.5, which means if the probability is larger than or equal to 0.5, the detected object is considered as rondel. Otherwise, it is regarded as an empty area (without rondel). For the test data set, there are 208 samples. Half of them are images with rondels, the other 104 samples are empty areas. As the model predicted, there should be 39 positive samples and 169 negative samples, of which there are 34 true positives, 99 true negatives, 5 false positives and 70 false negatives. The confusion matrix is shown as Table 5.3. Thus the precision is calculated by equation 4.3 as 87.17 %.

Initial learning rate	Batch size	Optimizer	Test Loss
0.01	16	SGD	0.0726
0.01	32	SGD	0.0411
0.01	64	SGD	0.0272
0.001	16	SGD	0.0352
0.001	32	SGD	0.0228
0.001	64	SGD	0.0883
0.0001	16	SGD	0.0509
0.0001	32	SGD	0.0269
0.0001	64	SGD	0.0407
0.0001	16	Adam	0.0895
0.0001	32	Adam	0.0519

Table 5.2: The different combinations of characteristics and their loss on test data. The model with lowest loss (best performance) is highlighted in yellow.

Actual \ Predicted	Positive	Negative
	Positive	TP = 34
Negative	FP = 5	TN = 99

Table 5.3: The confusion matrix (When the threshold is 0.5).

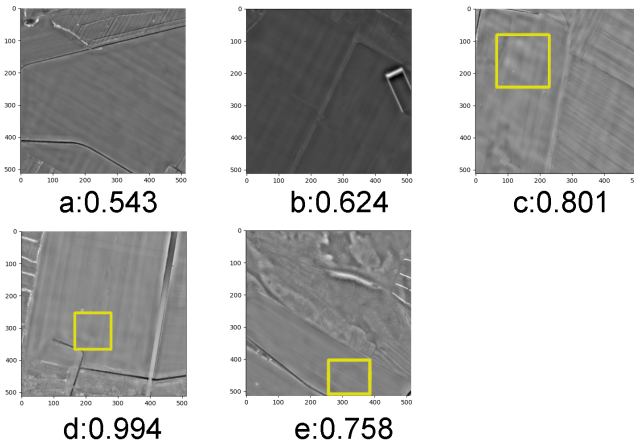


Figure 5.4: The false positives (The yellow boxes are drawn manually to emphasize the rondel-like patterns' location, the positions of the patterns can also be changed based on different people's judgment).

As discussed in Section 4.6, a low number of false positives is essential for the project. The 5 false positive samples in alphabetical order from a to e are shown in Figure 5.4. In image c,d and e, small circle patterns can be recognized. Yellow boxes were drawn

to emphasize the patterns. These patterns look similar to the rondel patterns. That explains why the model identified them as images with rondels. For the other 2 images – a and b, they have no distinguished rondel-like pattern. They are regarded as "negative" erroneous judgments of the model because it looks irrational.

On the other hand, according to the 5 samples, 0.5 might not be the best threshold in this case, because the probabilities of the 3 samples with rondel-like patterns are greater than 0.75. If the threshold was set as 0.75, the results might be more reasonable. In these circumstances, there should be 27 positive samples and 181 negative samples, of which there are 24 true positives, 101 true negatives, 3 false positives and 80 false negatives. The confusion matrix is shown as Table 5.4. The precision is calculated by equation 4.3 as 88.89 %, which shows a significant precision improvement compared to the 87.17 % when the threshold was 0.5.

Actual \ Predicted	Positive	Negative
	Positive	TP = 24
Negative	FP = 3	TN = 101

Table 5.4: The confusion matrix (When the threshold is 0.75).

It should be emphasized that all the discussion above was based on the hypothesis that all rondels in the area have already been detected and there were no more rondels. In fact, however, it can't be guaranteed according to the existing information. This leads to unknown error because of the difference between actual condition and the assumption.

5.4. SPATIAL DISTRIBUTION OF THE PREDICTION RESULTS AND DISCUSSION

After applying the best model on the LOT05 area, the probability map is shown in Figure 5.5. The base map of the figure is a topographical map.

According to the comparison between elevation map 4.6 and the probability distribution map in Figure 5.5, it is obvious that the probabilities have small values in the low-lying area and large values in the high-elevation area. This corresponds with the fact that all 7 rondels in LOT05 are located in the area with the higher elevation.

Figure 5.6 shows the probabilities distribution on a satellite map.

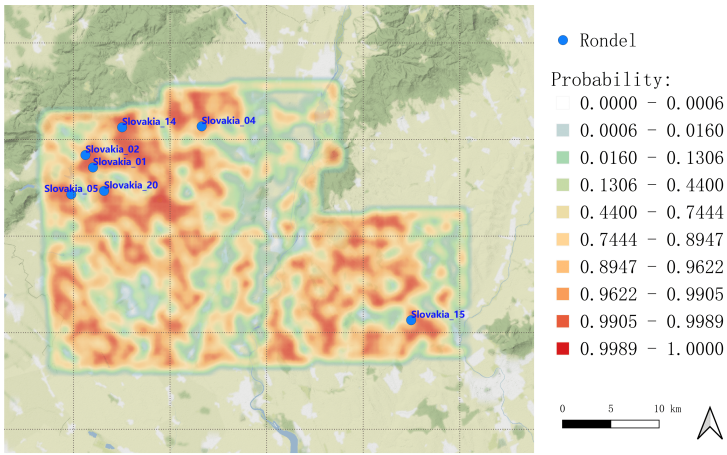


Figure 5.5: The spatial distribution of the probabilities of LOT05 on a topography map.

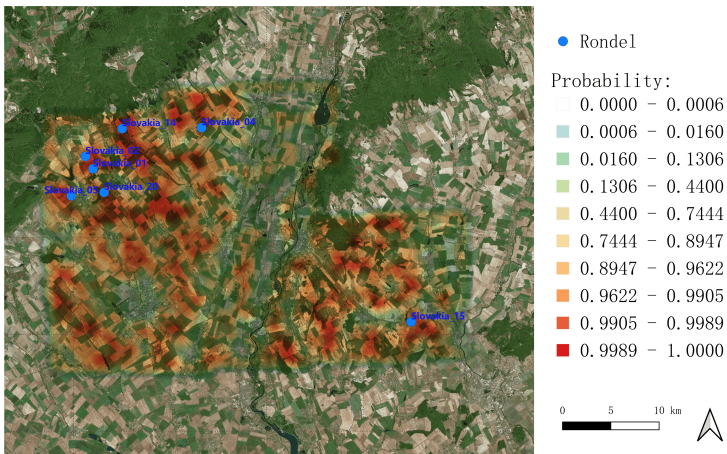


Figure 5.6: The spatial distribution of the probabilities of LOT05 on a satellite map.

In these figures, it is obvious that the distribution is inextricably linked with geography. Most of the low probability samples gather around the main river called Váh [45], the gullies and the residential areas, which can also be seen in Figure 5.7 and Figure 5.8.

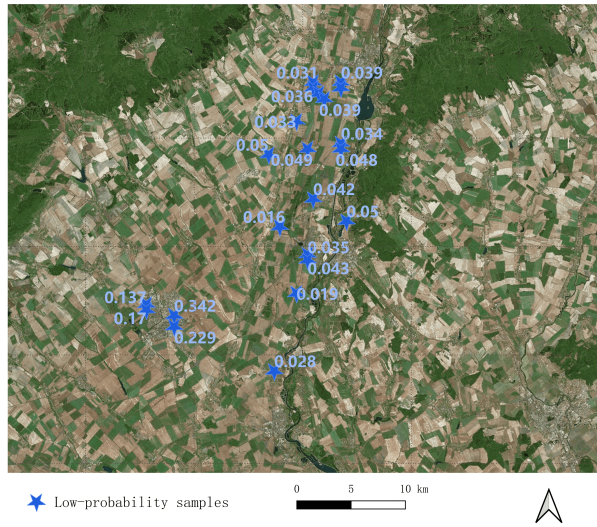


Figure 5.7: The area with low probability samples.



Figure 5.8: Zoom-in map with low probability samples.

As for samples with high probabilities, most of them are located in farming areas, as shown in Figure 5.9. According to the satellite map, it can be clearly seen that the abandoned river traces in these areas have become farming lands now (Figure 5.10). That's why it is inferred that the rondels might be built along the ancient river flows.

This hypothesis is further strengthened according to the positions of rondels in the areas besides LOT05 (Figure 5.11). There is another possibility that the known rondels all appear to be in rural areas or farmland because all the ones that were in more urban areas were already destroyed by human activity. Ergo, the only ones that we see are in relatively untouched areas such as farmlands.

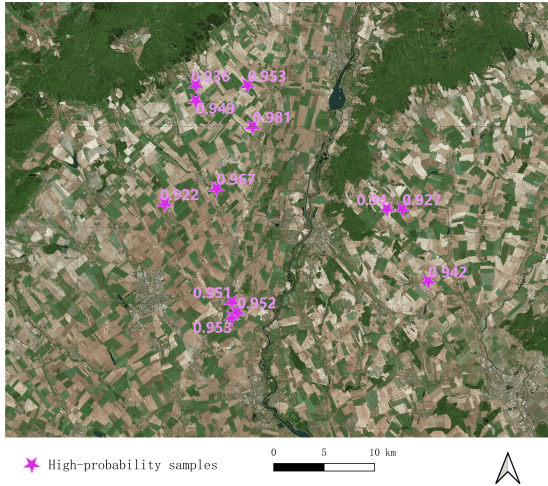


Figure 5.9: The area with high-probability samples.



Figure 5.10: The zoom-in map with high-probability samples.

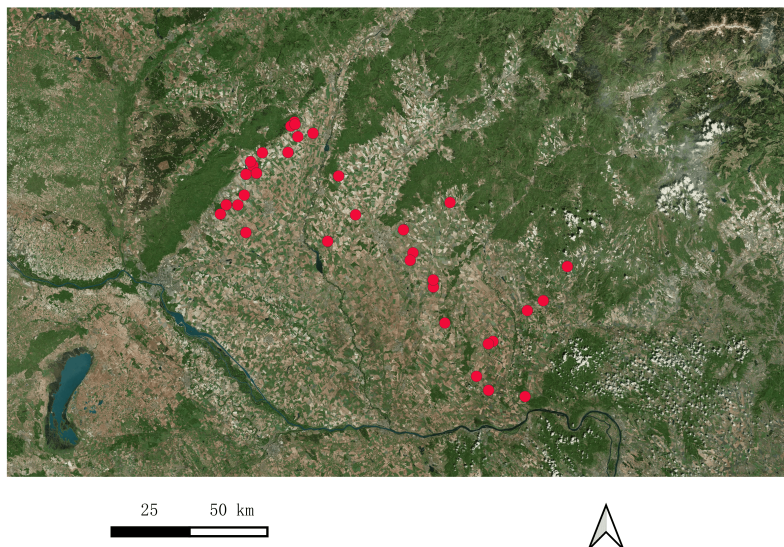


Figure 5.11: The positions of known rondels in Slovakia.

5.5. POSSIBLE NEW RONDELS

According to the model application on LOT5, 3982 possibilities were given out. Each of them represented the probability of the rondel existence on a $512 \times 512 \text{ m}^2$ area. After that, the areas were ordered from highest probability to lowest. Then the images with high probabilities were selected by the naked eyes according to the list. Finally, among the application with high probabilities, 32 possible new rondel areas, which are shown in Figure 5.12, Figure 5.13 and Table 5.5, were chosen to be further validated by archaeologists. Figures 5.14 and 5.15 show example images of 19th and 31st possible new rondels on the Google Map. In the middle of the figures, there are circle-like patterns on the ground, which are very likely to be new rondels. That's why the results are regarded to be useful to archaeological research in the future.

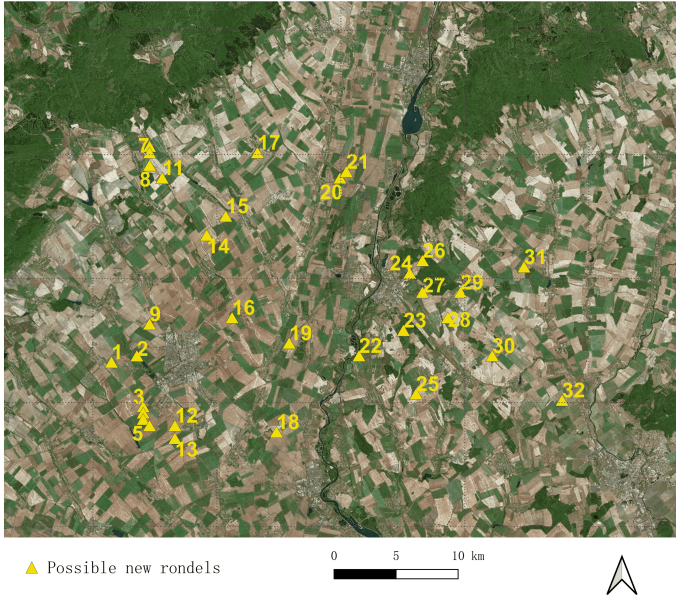


Figure 5.12: Locations of possible new rondels.

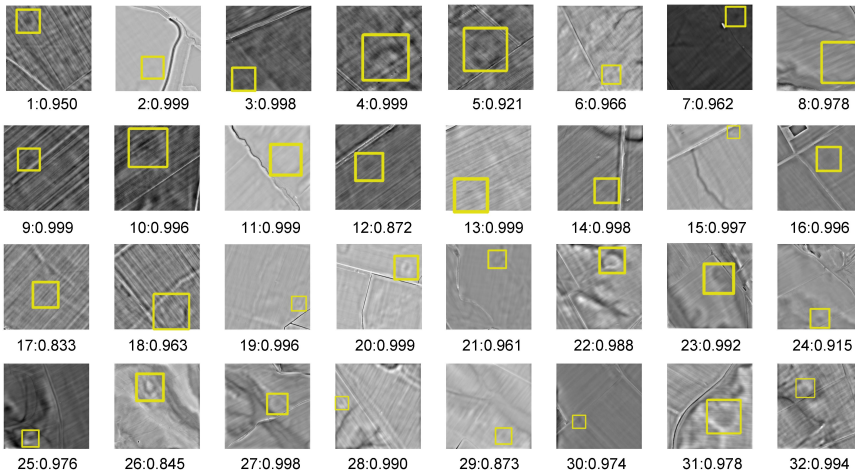


Figure 5.13: Images of possible new rondels and their probabilities in LOT05. All of them are 512 × 512 pixels (The yellow boxes are drawn manually to emphasize the rondel-like patterns' location, the positions can also be changed based on different people's judgment).

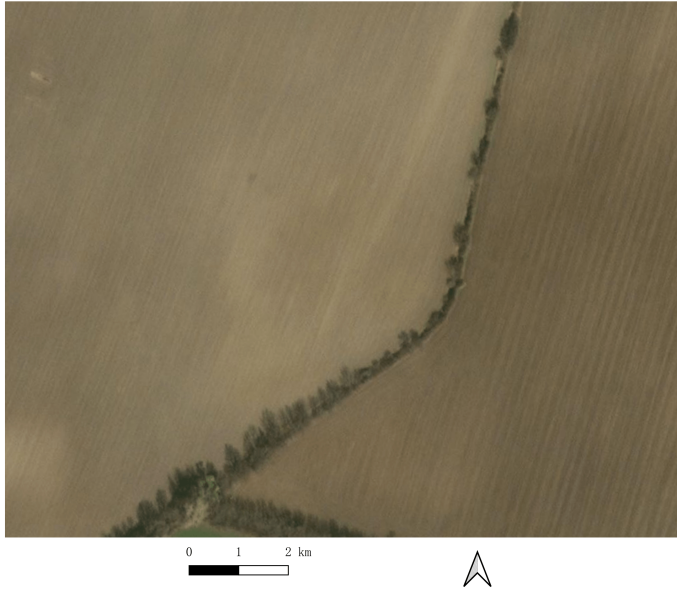


Figure 5.14: The 19th potential rondel shown on the Google Map.

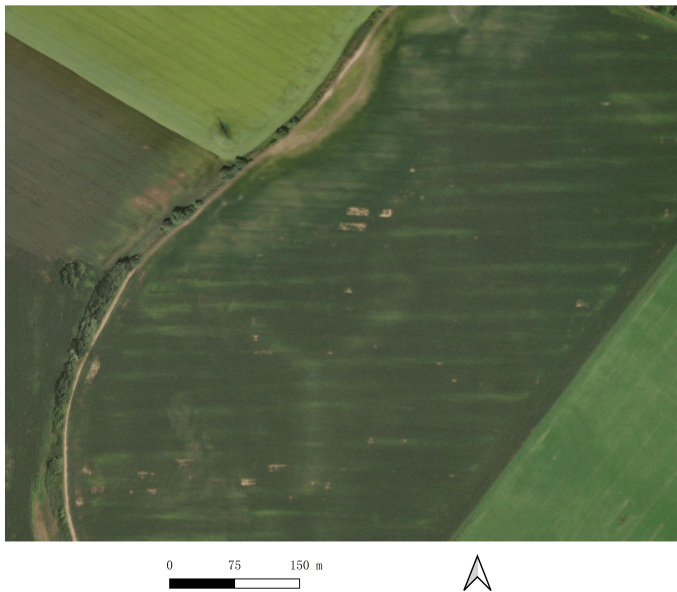


Figure 5.15: The 31st potential rondel shown on the Google Map.

index	X coordinate	Y coordinate	probability
1	241498	5363106	0.950
2	243546	5363618	0.999
3	244058	5359522	0.998
4	244058	5359010	0.999
5	244058	5358498	0.920
6	244570	5380514	0.965
7	244570	5380002	0.962
8	244570	5378978	0.967
9	244570	5366178	0.999
10	244570	5357986	0.995
11	245594	5377954	0.999
12	246618	5357986	0.872
13	246618	5356962	0.999
14	249178	5373346	0.998
15	250714	5374882	0.997
16	251226	5366690	0.996
17	253274	5380002	0.833
18	254810	5357474	0.963
19	255834	5364642	0.996
20	259930	5377954	0.999
21	260442	5378466	0.961
22	261466	5363618	0.988
23	265050	5365666	0.992
24	265562	5370274	0.915
25	266074	5360546	0.976
26	266586	5371298	0.845
27	266586	5368738	0.998
28	268634	5366690	0.990
29	269658	5368738	0.873
30	272218	5363618	0.974
31	274778	5370786	0.978
32	277850	5360034	0.994

Table 5.5: The list of possible new rondels. The coordinate system is EPSG:3046 - ETRS89 (meter).

5.6. RESULTS OF THE COMPARISON GROUP (EVALUATE THE USEFULNESS OF DATA AUGMENTATION)

The previous training steps were applied again on the comparison data set – data set without augmented rondels. Then the new model was used for predicting the probabilities of 32 possible rondels. The contrast of these two probabilities is shown in Table 5.6.

According to the results, there were 6 samples that shows distinguished probabiltieis reduction after the new-model application (Figure5.16). The new model failed to give higher probabilities to these 6 images. On the other hand, 5 samples were predicted 100 % as rondels. It might be concluded from this that the model based on the data set without augmentation showed more extreme and worse results. So the data augmentation was a necessary step.

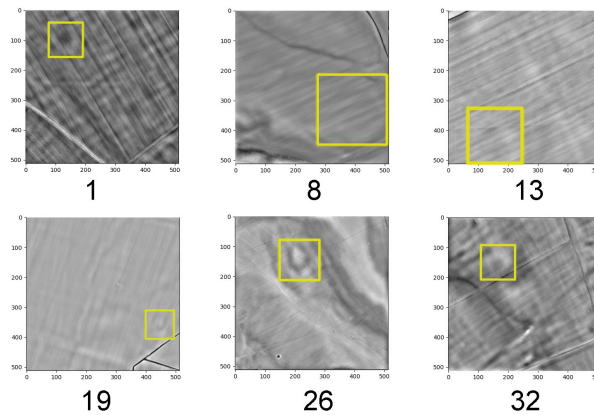


Figure 5.16: The 6 samples which show distinguished change after the new-model application (The yellow boxes are drawn manually to emphasize the rondel-like patterns' location, the positions can also be changed based on different people's judgment).

index	probability (original)	probability (without augmentation)
1	0.951	0.216
2	0.999	1
3	0.998	0.999
4	0.999	0.999
5	0.921	0.983
6	0.966	0.873
7	0.962	1
8	0.968	0.057
9	0.999	1
10	0.996	1
11	0.999	0.999
12	0.872	0.994
13	0.999	0.585
14	0.998	0.960
15	0.997	0.984
16	0.996	0.986
17	0.833	0.998
18	0.963	0.863
19	0.996	0.581
20	0.999	0.999
21	0.961	0.999
22	0.988	0.996
23	0.992	0.996
24	0.915	0.998
25	0.976	1
26	0.845	0.638
27	0.998	0.875
28	0.990	0.997
29	0.873	0.890
30	0.974	0.997
31	0.978	0.999
32	0.994	0.720

Table 5.6: The list of two probabilities of the possible rondels. The samples with significant different possibilities are highlighted in blue.

6

CONCLUSION & RECOMMENDATION

6.1. CONCLUSION (ANSWERS TO THE RESEARCH QUESTIONS)

In the following paragraphs, the answers to the research questions are given. The recommendations for future work are also put forward according to the conclusion of the previous work on this research.

- **What are the characteristics of rondels in images acquired by LiDAR?**

Most of the rondels have the common original structure, but were damaged because of plowing and construction activities. Nowadays they show the ring or part of the ring patterns on the images acquired by LiDAR, which have significant height difference because of the fences of the rondels. The size of the circle are varying from dozens of meters to 200 meters in diameter. These characteristics can be used to discriminate them from surface features on the images.

- **How can we train a good NCEs detector given the small size of the training data set?**

The training data set was expanded using augmentation. The detailed data augmentation steps are introduced in section 3.3 and section 4.2. According to the results comparison in section 5.6, the smaller data set without augmentation shows extreme results.

- **What is a good way to measure the performance of the classifier?**

The Cross-Entropy Loss Function was used to evaluate the model performance. Lower value of loss represents better performance of the model. On the other hand, setting a threshold on the probabilities that were given out by the deep learning method and using the confusion matrix can evaluate the classification results on the test data set.

- **How does the performance vary depending on how the network was trained?**

The different combinations of the characteristics were applied during the training process. The different performances of the models on the test data set can be seen in Figures 5.3 and Table 5.2. According to the loss evaluation, the 32 batch-size model shows a lower loss compared with the ones with 16 and 64 batch-size. For models with 0.01, 0.001 and 0.0001 initial learning rate values, the model with 0.001 shows the best performance. In the meanwhile, the model with the Stochastic Gradient Descent (SGD) optimizer shows a more stable performance in the process rather than the Adam optimizer. To sum up, the model with 32 batch-size, 0.001 initial learning rate and SGD optimizer shows the lowest loss, which means the best performance on test data set among the 11 models.

- **What's the performance when the model applies to the larger areas?**

The best model was applied to the area which was numbered LOT05 in Slovakia. Most known rondels are located on this area. On the map, the probability distribution has an obvious link to geomorphological characteristics, especially the flow of water trace. According to the high probabilities, several samples were selected for further validation. If some of them can be confirmed as a newly discovered rondel, the model can be regarded as a useful one.

- **Can new NCEs be detected using this method?**

It is hard to draw such a conclusion. According to the results for now, there are still interference factors, especially the changes of the environment caused by human and natural activities. The spatial distribution of the results can provide archaeologists and enthusiasts with positive assistance in future archaeological detection work and the high-probability samples are worth further validation.

6.2. RECOMMENDATION FOR FUTURE WORK

In order to provide a reference for future work, the recommendations or assumptions are given from the following aspects:

- **Type of data set** The data type used in this project is the elevation raster data derived from airborne LiDAR data. According to investigation from the archaeologists, the crop growth situation inside the rondels is different from the ones outside. That's why it might be a good choice if we use multi-spectral data like Sentinel-2 data to detect the crop growth situation. The multi-spectral data is a very efficient data type for plant research, based on the various combinations of the spectral bands. Moreover, fusing the height data and thermal data also has great potential. On the other hand, some of the known rondels are not visible because of the damage to their ground structures over the course of millennia and the low resolution of the measuring instrument. But the foundations of them should be left on the subsurface. The data which reflects characteristics of the subsurface is also worth trying in the future, such as the data from Synthetic Aperture Radar (SAR data) [46]. Even different combinations of data type can be used to get better models.

- **Size of data set** During the research process, data augmentation is one of the most essential parts. Finally, 421 augmented rondels were created based on 20 real rondels which were selected by naked eye. In the future, more augmented rondels can be created based on the augmentation methods. And research investigation moves forward, these will be more known positive samples. On the other hand, 3D augmented rondels might also be created using the point cloud data. The larger training data set for CNNs stands a good chance of resulting in a better performance of the results.
- **Visualization techniques** In the study, the Simple Local Relief Model was used for visualization. This visualization technique is a useful model for archaeological prospection, there should be more techniques. Some of them might be more efficient for this project, such as Multi-scale topographic position [47]. Moreover, some of them could also be stacked to realize better visualization results.
- **Improvement of the network** As for the construction and parameters of convolutional neural networks, there are lots of attempts to improve the performance of the training results. ResNet18 was used for model training in this project. Another CNNs might also be used to detect rondels in the area. On the other hand, the multi-channel inputs can also be used to train better models based on different kinds of data types or visualization techniques.

BIBLIOGRAPHY

- [1] Emilia Pásztor, Judit P Barna, and Georg Zotti. “Neolithic circular ditch systems (“Rondels”) in Central Europe”. In: *Handbook of archaeoastronomy and ethnoastronomy* (2015), pp. 1317–1326.
- [2] Georg Zotti and Wolfgang Neubauer. “Astronomical aspects of Kreisgrabenanlagen (Neolithic circular ditch systems)—an interdisciplinary approach”. In: *Proceedings of the International Astronomical Union 7.S278* (2011), pp. 349–356.
- [3] Wolfgang Sauber. *Museum Quintana. Neolithic wooden circular ditch (4840-4590 BC) in Künzing-Unternberg (reconstruction)*. URL: https://upload.wikimedia.org/wikipedia/commons/thumb/b/ba/Museum_Quintana_-_Unternberg_1.jpg/800px-Museum_Quintana_-_Unternberg_1.jpg (visited on 06/07/2009).
- [4] Alexandre Guyot et al. “Combined detection and segmentation of archeological structures from LiDAR data using a deep learning approach”. In: *Journal of Computer Applications in Archaeology* 4.1 (2021), p. 1.
- [5] Peter M Atkinson. “Autologistic regression for flood zonation using SAR imagery: proceedings of the 26th Annual Conference of the Remote Sensing Society 12-14th September 2000”. In: (2000).
- [6] Nicholas R Goodwin, Nicholas C Coops, and Darius S Culvenor. “Assessment of forest structure with airborne LiDAR and the effects of platform altitude”. In: *Remote Sensing of Environment* 103.2 (2006), pp. 140–152.
- [7] Anshuman Bhardwaj et al. “LiDAR remote sensing of the cryosphere: Present applications and future prospects”. In: *Remote Sensing of Environment* 177 (2016), pp. 125–143.
- [8] Leah A Wasser. “The basics of lidar-light detection and ranging-remote sensing”. In: *NSF NEON| Open Data to Understand our Ecosystems* 22 (2020).
- [9] Arlen F Chase et al. “Geospatial revolution and remote sensing LiDAR in Mesoamerican archaeology”. In: *Proceedings of the National Academy of Sciences* 109.32 (2012), pp. 12916–12921.
- [10] Øivind Due Trier, David C Cowley, and Anders Ueland Waldeland. “Using deep neural networks on airborne laser scanning data: Results from a case study of semi-automatic mapping of archaeological topography on Arran, Scotland”. In: *Archaeological Prospection* 26.2 (2019), pp. 165–175.
- [11] Eric Prehn. “Technical report: AIARCH Project Status - Searching for Neolithic Circular Enclosures”. In: (2021).
- [12] Žiga Kokalj and Ralf Hesse. “Airborne laser scanning raster data visualization”. In: *A guide to good practice* (2017).

- [13] Ioana Vizireanu and Răzvan Mateescu. “The potential of airborne LiDAR for detection of new archaeological site in Romania”. In: *Diversity in Coastal Marine Sciences: Historical Perspectives and Contemporary Research of Geology, Physics, Chemistry, Biology, and Remote Sensing* (2018), pp. 617–630.
- [14] Oliver Davis. “Processing and working with LiDAR data in ArcGIS: a practical guide for archaeologists”. In: (2012).
- [15] Tzelepis Nikos. *Formation of a hill-shading image*. URL: http://users.ntua.gr/bnakos/Hillshading_Eng.html.
- [16] David C Cowley. “Remote sensing for archaeology and heritage management—site discovery, interpretation and registration”. In: *EAC Occasional Paper No. 5 Occasional Publication of the Aerial Archaeology Research Group No. 3* (2011), p. 43.
- [17] Amy E Thompson. “Detecting classic Maya settlements with lidar-derived relief visualizations”. In: *Remote Sensing* 12.17 (2020), p. 2838.
- [18] Holley Moyes and Shane Montgomery. “Mapping ritual landscapes using Lidar: Cave detection through local relief modeling”. In: *Advances in Archaeological Practice* 4.3 (2016), pp. 249–267.
- [19] Yann LeCun, Yoshua Bengio, and Geoffrey Hinton. “Deep learning”. In: *nature* 521.7553 (2015), pp. 436–444.
- [20] Tahsin Mayeasha. *Getting Tensorflow, Theano and Keras on Windows*. 2016. URL: <https://medium.com/learning-machine-learning/getting-tensorflow-theano-and-keras-on-windows-70c18f2c533b>.
- [21] Ian Goodfellow, Yoshua Bengio, and Aaron Courville. *Deep learning*. MIT press, 2016.
- [22] The Click Reader. *Introduction to Convolutional Neural Networks*. 2022. DOI: <https://www.theclickreader.com/introduction-to-convolutional-neural-networks/>.
- [23] Gino Caspari and Pablo Crespo. “Convolutional neural networks for archaeological site detection—Finding “princely” tombs”. In: *Journal of Archaeological Science* 110 (2019), p. 104998.
- [24] Lihi Gur Arie. “The practical guide for object detection with YOLOv5 algorithm”. In: *The Practical Guide for Object Detection with YOLOv5 Algorithm* (2022).
- [25] Iason Katsamenis et al. “TraCon: A novel dataset for real-time traffic cones detection using deep learning”. In: *Novel & Intelligent Digital Systems: Proceedings of the 2nd International Conference (NiDS 2022)*. Springer. 2022, pp. 382–391.
- [26] Joseph Redmon et al. “You only look once: Unified, real-time object detection”. In: *Proceedings of the IEEE conference on computer vision and pattern recognition*. 2016, pp. 779–788.
- [27] Kaiming He et al. “Deep residual learning for image recognition”. In: *Proceedings of the IEEE conference on computer vision and pattern recognition*. 2016, pp. 770–778.

- [28] Farheen Ramzan et al. “A deep learning approach for automated diagnosis and multi-class classification of Alzheimer’s disease stages using resting-state fMRI and residual neural networks”. In: *Journal of medical systems* 44 (2020), pp. 1–16.
- [29] Paolo Napoletano, Flavio Piccoli, and Raimondo Schettini. “Anomaly detection in nanofibrous materials by CNN-based self-similarity”. In: *Sensors* 18.1 (2018), p. 209.
- [30] Qiming Zhou. “Digital elevation model and digital surface model”. In: *International Encyclopedia of Geography: People, the Earth, Environment and Technology* (2017), pp. 1–17.
- [31] Cartography 2020 Office of Geodesy and Cadastre of the Slovak Republic. ÚGKK SR. URL: <https://www.skgeodesy.sk/sk/ugkk/> (visited on 07/15/2021).
- [32] Ujaval Gandhi. “QGIS Tutorials and Tips”. In: *Retrieved January 20* (2001).
- [33] Zoran Čučković. *Hillshade in QGIS: how does it work?* URL: <https://landscapearchaeology.org/2020/hillshade/>.
- [34] *Hillshade*. URL: <http://www.geography.hunter.cuny.edu/~jochen/gtech361/lectures/lecture11/concepts/hillshade.htm>.
- [35] Sphinx and pradyunsg’s Furo. *Relief Visualization Toolbox – Visualization Functions*. URL: <https://rvt-py.readthedocs.io/en/latest/rvt.vis.html>.
- [36] Ron Kohavi et al. “A study of cross-validation and bootstrap for accuracy estimation and model selection”. In: *International Joint Conference on Artificial Intelligence*. Vol. 14. 2. Montreal, Canada. 1995, pp. 1137–1145.
- [37] Jahnvi Thekkada. *Is Balancing the Imbalanced Data important in ML*. URL: <https://www.linkedin.com/pulse/balancing-imbalanced-data-important-ml-jahnvi-thekkada>.
- [38] Qiong Wei and Roland L Dunbrack Jr. “The role of balanced training and testing data sets for binary classifiers in bioinformatics”. In: *PloS one* 8.7 (2013), e67863.
- [39] Nagdev Amruthnath. *Why balancing your data set is important?* URL: <https://www.r-bloggers.com/2020/06/why-balancing-your-data-set-is-important/>.
- [40] Sagar Imambi, Kolla Bhanu Prakash, and GR Kanagachidambaresan. “PyTorch”. In: *Programming with TensorFlow: Solution for Edge Computing Applications* (2021), pp. 87–104.
- [41] Michael A Nielsen. *Neural networks and deep learning*. Vol. 25. Determination press San Francisco, CA, USA, 2015.
- [42] Nitish Shirish Keskar and Richard Socher. “Improving generalization performance by switching from Adam to SGD”. In: *arXiv preprint arXiv:1712.07628* (2017).
- [43] Li Li, Miloš Doroslovački, and Murray H Loew. “Approximating the gradient of cross-entropy loss function”. In: *IEEE Access* 8 (2020), pp. 111626–111635.

- [44] Mutegeki Ronald, Alwin Poullose, and Dong Seog Han. “iSPLInception: An inception-ResNet deep learning architecture for human activity recognition”. In: *IEEE Access* 9 (2021), pp. 68985–69001.
- [45] Katarina Jeneiová, Silvia Kohnová, and Miroslav Sabo. “Detecting trends in the annual maximum discharges in the Vah River Basin, Slovakia”. In: *Acta Silvatica et Lignaria Hungarica* 2010.2 (2014), pp. 131–142.
- [46] Richard Bamler. “Principles of synthetic aperture radar”. In: *Surveys in Geophysics* 21.2 (2000), pp. 147–157.
- [47] JB Lindsay, JMH Cockburn, and HAJ Russell. “An integral image approach to performing multi-scale topographic position analysis”. In: *Geomorphology* 245 (2015), pp. 51–61.

A

APPENDIX

A.1. THE ARCHITECTURE OF RESNET18

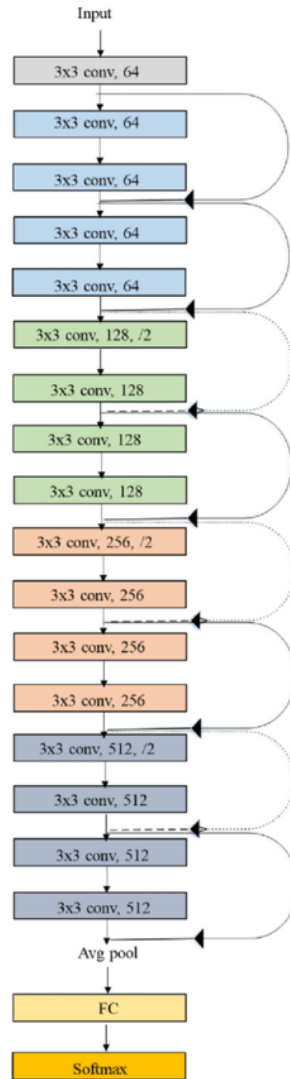


Figure A.1: The architecture of ResNet18 [28].

A.2. THE LIST OF ACRONYM

Acronym	Full Name
NCE	Neolithic Circular Enclosures
SLRM	Simple Local Relief Model
LiDAR	Light Detection And Ranging
CNN	Convolutional Neural Networks
DTM	Digital Terrain Model
DSM	Digital Surface Model
GSD	Ground Sampling Distance
ResNet	Residual Network
SGD	Stochastic Gradient Descent
Adam	Adaptive moment estimation

Table A.1: Acronym list